

On the pole trajectory of the subthreshold negative parity nucleon with varying pion masses

Qu-Zhi Li,^{*} Zhiguang Xiao,[†] and Han-Qing Zheng[‡]
College of Physics, Sichuan University, Chengdu 610065, P. R. China

We study the pole trajectory of the recently established subthreshold negative parity nucleon, namely the $N^*(920)$, with varying pion masses, in the scheme of linear σ model with nucleons. We find that the pole moves from the complex plane to the real axis rather straightforwardly, on the second Riemann sheet. We also re-examined the σ pole trajectory and find it in good agreement with Roy equation analysis result.

I. INTRODUCTION

A subthreshold pole with quantum number $J^{PC} = 1/2^-$, named $N^*(920)$, has been established in the S_{11} channel of πN scatterings in recent years. It has been firstly noticed in analyzing πN scattering data [1, 2] using the product representation for partial wave amplitudes [3–5], which comes from the correct treatment of the left hand cuts and unitarization [6, 7]. The pole is also confirmed using naive K -matrix approach [8] and N/D method [9]. Its existence is firmly established in a Roy-Steiner equation analysis in Ref. [10], with the pole location $\sqrt{s} = (918 \pm 3) - i(163 \pm 9)$ GeV, and is reconfirmed in Ref. [11]. Hence there is no doubt on the very existence of $N^*(920)$ pole. Its properties in turn naturally become a subject of research interest, since much is left to be desired.

The early work on the properties of $N^*(920)$ is its coupling to $N\gamma$ and $N\pi$ [12]. It is found that its coupling to $N\pi$ is considerably larger than that of $N^*(1535)$, while its coupling to $N\gamma$ is comparable to that of $N^*(1535)$. Here in this note we will focus on the $N^*(920)$ pole trajectory with varying pion masses.

In the literature, the σ pole trajectory with varying π masses has been a rather hot topic for discussions, see for example Refs. [13, 14] and references therein. Remarkably a model independent Roy equation analysis has been carried out to thoroughly solve the issue [15]. The study of the σ pole trajectory with varying m_π is important, since it opens a new window in understanding non-perturbative strong interaction physics provided by lattice QCD calculations. An alternative study based on $O(N)$ linear σ model [16, 17] finds similar results comparing with that of Ref. [15], hence providing further evidence that the σ meson may be more reasonably described as “elementary”, in the sense that it is, the same as pions, described by an explicit field degree of freedom in the effective chiral lagrangian¹. Inspired by this, we in this paper adopt the effective lagrangian with a linearly realized chiral symmetry. To be specific we use the renormalizable linear σ model with nucleon fields, though it is known that renormalizability condition is not at all a physical requirement when describing low energy hadron physics.

In the following we begin by a brief introduction of the linear σ model with nucleons in Sec. II, and calculate the σ pole trajectory using [1,1] Padé approximation in Sec. III. As it is verified that the unitarity approximation does give a similar σ pole trajectory as comparing with that of Ref. [15], it is satisfactory to use the same approximation method to further explore the $N^*(920)$ trajectory, which will also be discussed in Sec. III. Sec. IV is devoted to discussions and conclusions.

II. A BRIEF REVIEW OF LINEAR σ MODEL

The linear σ model [21] (LSM) lagrangian with a nucleon field can be written as follows:

$$\begin{aligned} \mathcal{L} = & \bar{\Psi}_0 i \gamma^\mu \partial_\mu \Psi_0 - g_0 \bar{\Psi}_0 (\sigma_0 + i \gamma_5 \vec{\tau} \cdot \boldsymbol{\pi}_0) \Psi \\ & + \frac{1}{2} (\partial_\mu \sigma_0 \partial^\mu \sigma_0 + \partial_\mu \boldsymbol{\pi}_0 \cdot \partial^\mu \boldsymbol{\pi}_0) - \frac{\mu^2}{2} (\sigma_0^2 + \boldsymbol{\pi}_0^2) - \frac{\lambda_0}{4!} (\sigma_0^2 + \boldsymbol{\pi}_0^2)^2 + C \sigma_0, \end{aligned} \quad (1)$$

^{*} liquzhi@scu.edu.cn

[†] xiaozg@scu.edu.cn

[‡] zhenghq@pku.edu.cn

¹ Early studies using large N_c (number of colors) arguments also support such a suggestion [18–20].

where Ψ_0 is the isospin doublet denoting bare nucleon fields, and $\boldsymbol{\pi}_0, \sigma_0, \mu_0, g_0, \lambda_0$ are bare π meson triplet, σ field, a mass parameter, and couplings, respectively. The renormalized quantities are related to bare ones through:

$$\begin{cases} \psi_0 = \sqrt{Z_\psi} \psi, \\ (\sigma_0, \boldsymbol{\pi}_0) = \sqrt{Z_\phi} (\sigma, \boldsymbol{\pi}), \\ \mu_0^2 = \frac{1}{Z_\phi} (\mu^2 + \delta\mu^2), \\ g_0 = \frac{Z_g}{Z_\psi \sqrt{Z_\phi}} g, \\ \lambda_0 = \frac{Z_\lambda}{Z_\phi^2} \lambda. \end{cases} \quad (2)$$

Spontaneous chiral symmetry breaking (χ SB) occurs when the σ vacuum expectation value (vev) $\langle \sigma \rangle = v \neq 0$, generating three zero-mass Goldstone bosons: π^i , $i = 1, 2, 3$ in the absence of explicit χ SB term $C\sigma_0$. To make correct perturbation expansion one shifts $\sigma \rightarrow \sigma + v$ such that $\langle \sigma \rangle = 0$ and get,

$$\begin{aligned} \mathcal{L} = & \bar{\psi} [i\not{\partial} - m_N - g(\sigma + i\boldsymbol{\pi} \cdot \boldsymbol{\tau}\boldsymbol{\gamma}_5)] \psi \\ & + \bar{\psi} [-\delta m_N - \delta g(\sigma + i\boldsymbol{\pi} \cdot \boldsymbol{\tau}\boldsymbol{\gamma}_5) + i(Z_\psi - 1)\not{\partial}] \psi \\ & + \frac{1}{2} [(\partial_\mu \sigma)^2 + (\partial_\mu \boldsymbol{\pi})^2 - m_\sigma^2 \sigma^2 - m_\pi^2 \boldsymbol{\pi}^2 \\ & + (Z_\phi - 1) ((\partial_\mu \sigma)^2 + (\partial_\mu \boldsymbol{\pi})^2) - \delta m_\pi^2 \boldsymbol{\pi}^2 - \delta m_\sigma^2 \sigma^2] - \frac{\lambda}{4!} [\sigma^4 + \boldsymbol{\pi}^4 + 4v\sigma(\sigma^2 + \boldsymbol{\pi}^2) + 2\sigma^2 \boldsymbol{\pi}^2] \\ & - \frac{\lambda}{4!} (Z_\lambda - 1) [\sigma^4 + \boldsymbol{\pi}^4 + 4v\sigma(\sigma^2 + \boldsymbol{\pi}^2) + 2\sigma^2 \boldsymbol{\pi}^2] - \sigma [v(m_\pi^2 + \delta m_\pi^2) - C\sqrt{Z_\phi}], \end{aligned} \quad (3)$$

with

$$m_N = gv, \quad m_\sigma^2 = \mu^2 + \frac{1}{2}\lambda v^2, \quad m_\pi^2 = \mu^2 + \frac{1}{6}\lambda v^2, \quad (4)$$

and the renormalization constants are defined as

$$\begin{cases} \delta m_N = m_N(Z_g - 1), \\ \delta g = g(Z_g - 1), \\ \delta m_\pi^2 = \delta\mu^2 + \frac{1}{6}(Z_\lambda - 1)\lambda v^2, \\ \delta m_\sigma^2 = \delta\mu^2 + \frac{1}{2}(Z_\lambda - 1)\lambda v^2. \end{cases} \quad (5)$$

From Eq. (4) we obtain the relation between m_π and m_σ :

$$m_\sigma^2 = m_\pi^2 + \frac{1}{3}\lambda v^2. \quad (6)$$

This relation holds if the renormalization constant Z_λ is taken as

$$Z_\lambda = 1 - \frac{3(\delta m_\pi^2 - \delta m_\sigma^2)}{\lambda v^2}. \quad (7)$$

The other renormalization constants are determined by the following conditions, as done in Ref. [22]:

- For δm_π^2 and Z_ϕ , we demand that the full π propagator $\Delta_\pi(s)$ satisfies

$$\begin{aligned} i\Delta_\pi^{-1}(m_\pi^2) &= 0, \\ i \frac{d\Delta_\pi^{-1}(s)}{ds} \Big|_{s=m_\pi^2} &= 1. \end{aligned} \quad (8)$$

- δm_σ^2 can be determined by requiring the real part of the σ propagator, $i\Delta_\sigma^{-1}(s)$, to vanish when $s \rightarrow m_\sigma^2$, i.e.,

$$\text{Re}[i\Delta_\sigma^{-1}(m_\sigma^2)] = 0. \quad (9)$$

Notice that the parameter m_σ can not be identified as the σ pole mass when $m_\sigma > 2m_\pi$ since $i\Delta_\sigma^{-1}(m_\sigma^2)$ is complex in this situation. On the other hand, if m_π increases to be large enough such that $m_\sigma < 2m_\pi$, then $i\Delta_\sigma^{-1}(m_\sigma^2)$ becomes real and m_σ is just the pole mass.

- Z_ψ and Z_g are determined by forcing the full nucleon propagator $\Delta_N(\not{p})$ behaving like:

$$\begin{aligned} i\Delta_N^{-1}(m_N) &= 0, \\ i\frac{d\Delta_N^{-1}(\not{p})}{d\not{p}}\Big|_{\not{p}=m_N} &= 1. \end{aligned} \quad (10)$$

The results for the renormalization constants and counter terms under these renormalization conditions are listed in Appendix A.

In LSM, there are only four free parameters and they can be chosen as λ , m_σ , m_π , g . From Eqs. (6) and (4), the vev v and the nucleon mass m_N are expressed by:

$$v^2 = \frac{3(m_\sigma^2 - m_\pi^2)}{\lambda}, \quad m_N = gv. \quad (11)$$

In the physical situation, $m_\pi = 0.140\text{GeV}$, $m_N = 0.938\text{GeV}$, and v is identical to the pion decay constant f_π at tree level, whose experimental value is 0.093GeV so that $g \simeq 10$. From PCAC, one also obtains $C\sqrt{Z_\phi} = f_\pi m_\pi^2$, and the pion decay constant f_π are related to v by [23]:

$$v = f_\pi m_\pi^2 i\Delta_\pi(0). \quad (12)$$

Since our purpose of using the LSM is to approximate QCD which has fewer parameters than LSM, this will impose some constraints to the free parameters of LSM. One constraint from Lattice QCD is the dependence of f_π on m_π in Ref. [24] as shown in the left diagram of FIG. 1. As a good approximation, one can use a linear function to parameterize the lattice result:

$$f_\pi = km_\pi + b, \quad (13)$$

with $k \simeq 0.048$, $b \simeq 0.087\text{GeV}$. The intercept b denotes the value of f_π in the chiral limit $m_\pi \rightarrow 0$.

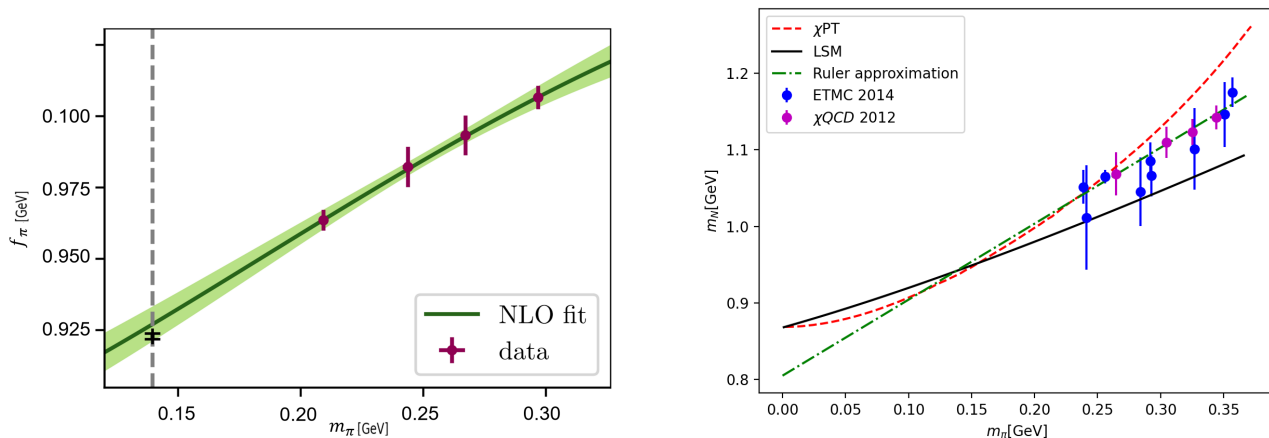


FIG. 1: Left: the dependence of pion decay constant on pion mass (figure from Ref. [24]); Right: nucleon mass dependence on pion mass. Data from χ QCD [25], ETMC [26], ruler approximation [27], χ PT [28–30].

Combining Eqs. (13) and (12), the relation between v and m_π can be obtained which is required for the study of $N^*(920)$ trajectory. At tree level, Eq. ((12)) simply means $f_\pi = v$. Remembering $m_N = gv$ we can reach a conclusion that m_N is also a linear function of m_π with slope gk and intercept gb assuming that g is independent of m_π . The full pion-mass dependence is shown in FIG. 1 compared with the χ PT prediction and lattice results. As depicted, the nucleon mass in LSM coincides with the result of χ PT in the chiral limit, which is larger than the prediction of “ruler approximation” [27]. For m_π ranging from the chiral limit to about 0.2GeV , the nucleon mass in LSM is close to the result of χ PT, while for m_π above 0.25GeV , the values match lattice data within a certain margin of error. This also justifies the assumption that g is independent of m_π .

Though π meson self-energy correction should be taken into account in Eq. (12) at one-loop level, the contributions from self-energy correction to v are negligible for m_σ ranging from 0.55GeV to 1.5GeV [22]. So the linear dependence of nucleon mass on m_π still holds at one-loop level.

With the pion mass dependence of v Eq. (12), from the first equation of (11), there are two alternative simple assumptions to choose in order to proceed: to fix m_σ such that λ is dependent on m_π or vice versa. Since the results of these two choices would produce similar qualitative results, we choose the first one in discussing the $\pi\pi$ scatterings and only provide the results in πN scatterings for both choices.

III. THE TRAJECTORIES OF THE σ POLE AND THE $N^*(920)$ POLE

This section is devoted to the study of the σ pole and the $N^*(920)$ pole dependence on varying pion masses. This analysis is meaningful in understanding the non-perturbative aspects of low energy strong interaction physics, especially in the era when lattice QCD studies become more and more prosperous² For the former, the σ pole trajectory is well understood [15, 32] while knowledge of $N^*(920)$ trajectory is absent yet, from either lattice QCD or analytical studies.

We will study the two trajectories based on the renormalizable linear σ model with nucleons. The reason why we choose such a model is already discussed in the introduction. We in the following firstly re-analyze the σ pole trajectory using [1,1] Padé approximation³. It will be found that the trajectory obtained is in good agreement with that of Roy equation analyses and the $O(N)$ model results qualitatively.

A. The σ pole location in the $I, J = 0, 0$ channel $\pi\pi$ scattering amplitude

Basically there can be two ways to extract the σ pole location: one is from the σ propagator, another is from the unitarized $\pi\pi$ scattering amplitude. They are not equivalent under the approximations being used, however. The propagator is obtained by using a Dyson resummation of self energy bubble chain, and is essentially a one loop calculation, whereas the pole in the unitarized amplitude contains more complete dynamical input⁴. Therefore we adopt the scattering amplitude to extract the pole locations.

The $\pi\pi$ elastic scattering amplitude is written as:

$$T(s, t, u) = A(s, t, u)\delta_{\alpha\beta}\delta_{\gamma\delta} + B(s, t, u)\delta_{\alpha\gamma}\delta_{\beta\delta} + C(s, t, u)\delta_{\alpha\delta}\delta_{\gamma\beta} \quad (14)$$

where α, β, γ and δ are isospin indexes and s, t and u are Mandelstam variables subject to the constraints $s + u + t = 4m_\pi^2$. $A(s, t, u), B(s, t, u)$ and $C(s, t, u)$ are Lorentz invariant amplitudes. The total isospin $I = 0$ amplitude $T^0(s, t, u)$ can be derived as

$$T^0(s, t, u) = 3A(s, t, u) + B(s, t, u) + C(s, t, u) . \quad (15)$$

The Feynman diagrams contributing to $\pi\pi$ scattering amplitudes are presented in FIG 2.

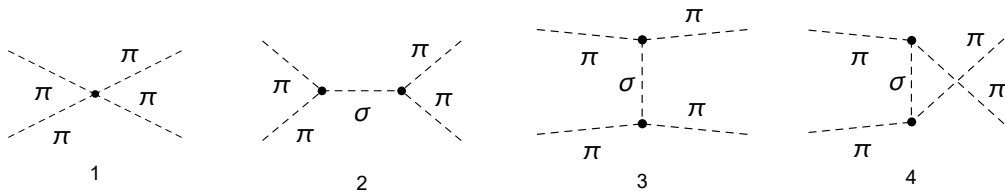


FIG. 2: The tree-level Feynman diagrams contributing to $\pi\pi$ scatterings.

² For a recent review to the related subjects, one is referred to Ref. [31].

³ It is not at all obvious that Padé approximation leads to a satisfied solution since it may be spoiled by spurious poles [33]. But in linear σ model it works rather good, since crossing symmetry is restored.

⁴ To be more specific, at one loop, the self energy on the second sheet contains the pseudo-threshold but not the dynamical left hand cut (the crossed channel σ exchanges), which is presented anyway in unitarized scattering amplitudes. So the two solutions cannot be the same.

The corresponding invariant amplitude $A(s, t, u)$ reads:

$$A(s, t, u) = -\frac{\lambda^2 v^2}{9(s - m_\sigma^2)} - \frac{\lambda}{3}. \quad (16)$$

The invariant amplitudes $B(s, t, u)$ and $C(s, t, u)$ are related to $A(s, t, u)$ via crossing symmetry:

$$A(s, t, u) = B(t, s, u) = C(u, t, s). \quad (17)$$

Partial wave amplitude(PWA) is defined as

$$T_J^I(s) = \frac{1}{32\pi(s - 4m_\pi^2)} \int_{4m_\pi^2 - s}^0 P_J \left(1 + \frac{2t}{s - 4} \right) T^I(s, t, u), \quad (18)$$

where P_J is the Legendre polynomial. The elastic unitarity reads:

$$\text{Im } T_J^I(s) = \rho(s, m_\pi, m_\pi) |T_J^I(s)|^2, \quad s > 4m_\pi^2, \quad (19)$$

with

$$\rho(s, m_1, m_2) = \frac{\sqrt{(s - (m_1 + m_2)^2)(s - (m_1 - m_2)^2)}}{s}. \quad (20)$$

The PWA has been calculated up to one-loop level within LSM neglecting nucleon contributions. From perturbative unitarity in LSM we have:

$$\text{Im } T_{0t}^0(s) = \rho(s, m_\pi, m_\pi) |T_{0t}^0(s)|^2, \quad 4m_\pi^2 < s < 4m_\sigma^2, \quad (21)$$

where $T_{0t}^0(s)$ and $T_{0l}^0(s)$ denote the tree-level and the one-loop PWAs, respectively. Combining Eq.(15)-(18), the tree-level PWA is obtained:

$$T_{0t}^0(s) = \frac{\lambda}{48\pi} \left(\frac{(3m_\pi^2 + 2m_\sigma^2 - 5s)}{2(s - m_\sigma^2)} + \frac{(m_\sigma^2 - m_\pi^2) \log \left(\frac{s - 4m_\pi^2 + m_\sigma^2}{m_\sigma^2} \right)}{(s - 4m_\pi^2)} \right). \quad (22)$$

At one-loop order, it is tedious to present all Feynman diagrams and their corresponding results, which exceed 50 diagrams [34]. Therefore, we will not include those amplitudes in this manuscript⁵. With Eq. (21), it is easy to prove that the [1, 1] Padé approximant

$$T_0^{0[1,1]}(s) = \frac{T_{0t}^0(s)}{1 - T_{0l}^0(s)/T_{0t}^0(s)}, \quad (23)$$

satisfies elastic unitarity. The σ resonance corresponds to the pole of the PWA on the second Riemann sheet (RSII) of complex s plane, or the zero of partial wave S matrix:

$$S(s) = 1 + 2i\rho(s, m_\pi, m_\pi) T_0^{0[1,1]}(s), \quad (24)$$

on the first Riemann sheet (RSI).

According to Eq. (23), the numerator of $T_0^{0[1,1]}(s)$, i.e., T_{0t}^0 , contains a first-order pole at m_σ^2 . When $m_\sigma > 2m_\pi$, in the denominator $1 - T_{0l}^0/T_{0t}^0$, there also exists a first-order pole because the loop-level amplitude $T_{0l}^0(s)$ contains a second-order pole at m_σ^2 from the one-loop σ propagator as shown in the right diagram of FIG. 3. This causes $T_0^{0[1,1]}(s)$ to be finite at m_σ^2 . Thus, in this situation m_σ is not the pole mass of σ and the σ pole position would lie on the second Riemann sheet. On the contrary, with m_π growing up to $2m_\pi > m_\sigma$, the second-order pole in $T_{0l}^0(s)$ transforms to a first-order pole because the residue being proportional to $\Sigma(m_\sigma^2)$ equals zero due to the reomormalization condition (8). In this case, the denominator of Eq. (23) is finite at m_σ^2 , and the numerator remains a pole at m_σ^2 which corresponds to the σ bound state.

⁵ The numerical code is available upon request.

With $m_\sigma = 0.7\text{GeV}$ and physical pion mass, the σ pole locates at about $(0.47 - i0.16)$ GeV, which is consistent with the PDG result. Fixing this m_σ parameter and taking into account the relation between f_π and m_π in (13), the trajectory of σ pole with increasing m_π is depicted in FIG. 3. The σ resonance falls down to real axis below the threshold from the complex plane above the threshold, becoming two virtual states (VS I and VS II) when m_π increases from physical value to $m_\pi \simeq 0.32\text{GeV}$. One of them (VS II) runs towards threshold and finally crosses the threshold to the real axis below the threshold on RSI, turning into a bound state when $2m_\pi > m_\sigma$. On the other hand, the other virtual state (VS I) runs away from the threshold and collides with the third virtual state (VS III) which appears from the left-hand cut when $m_\pi \simeq 0.22\text{GeV}$. Then these two virtual-state poles turn into a pair of resonance poles on the complex plane. The trajectory is similar to that of the Roy equation [35] the N/D modified $O(N)$ model [16], but now the critical point ($m_\sigma/2$) when σ becomes a bound state can be determined analytically from the expression of Padé amplitude.

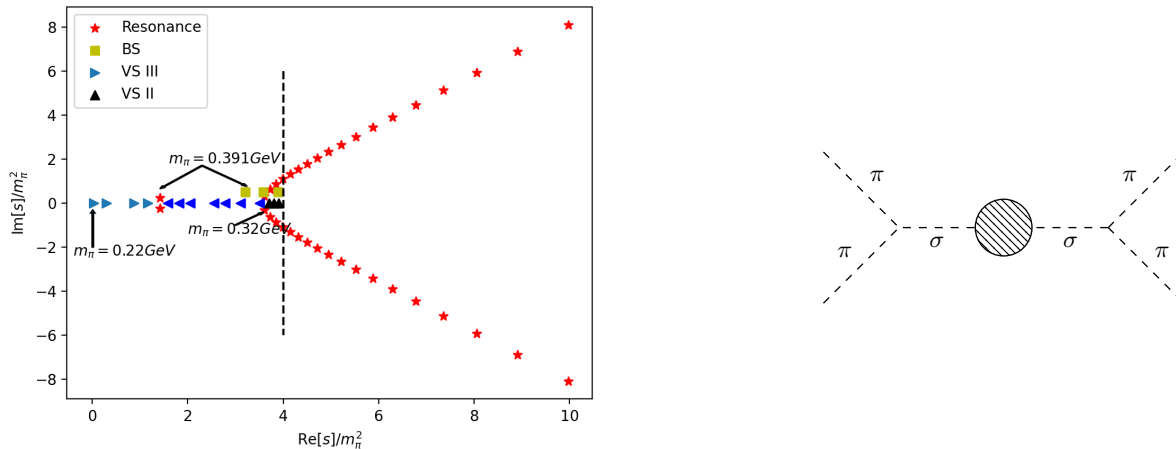


FIG. 3: The trajectory of σ resonance with m_π variation. Right: the contribution of σ self-energy correction to $\pi\pi$ amplitude.

Having examined that the σ pole trajectory can be satisfactorily reproduced in the scheme of linear σ model with Padé unitarization, we are confident to step forward by studying the $N^*(920)$ pole trajectory in the linear σ model with nucleon field, in the next subsection.

B. S_{11} channel of πN scattering amplitude

For the process $\pi^a(p) + N_i(q) \rightarrow \pi^{a'}(p') + N_f(q')$, the isospin amplitude can be decomposed as:

$$T = \chi_f^\dagger \left(\delta^{aa'} T^+ + \frac{1}{2} [\tau^{a'}, \tau^a] T^- \right) \chi_i, \quad (25)$$

where τ^a ($a = 1, 2, 3$) are Pauli matrices, and χ_i (χ_f) corresponds to the isospin wave function of the initial (final) nucleon state. The amplitudes with isospins $I = 1/2, 3/2$ can be written as

$$\begin{aligned} T^{I=1/2} &= T^+ + 2T^-, \\ T^{I=3/2} &= T^+ - T^-. \end{aligned} \quad (26)$$

As for Lorentz structure, for an isospin indices $I = 1/2, 3/2$,

$$T^I = \bar{u}^{(s')} (q') \left[A^I(s, t) + \frac{1}{2} (\not{p} + \not{p}') B^I(s, t) \right] u^{(s)}(q), \quad (27)$$

with the superscripts $(s), (s')$ denoting the spins of Dirac spinors and three Mandelstam variables $s = (p + q)^2, t = (p - p')^2, u = (p - q')^2$ obeying the constraint $s + t + u = 2m_N^2 + 2m_\pi^2$. The channel with orbit angular momentum L ,

total angular momentum J and total isospin I denoted as $T(L_2 I_2 J)$ is defined as:

$$T_{\pm}^{I,J} = T(L_2 I_2 J) = T_{++}^{I,J}(s) \pm T_{+-}^{I,J}(s), \quad L = J \mp \frac{1}{2}, \quad (28)$$

where the definition of partial wave helicity amplitudes are written as:

$$\begin{aligned} T_{++}^{I,J} &= 2m_N A_C^{I,J}(s) + (s - m_\pi^2 - m_N^2) B_C^{I,J}(s) \\ T_{+-}^{I,J} &= -\frac{1}{\sqrt{s}} \left[(s - m_\pi^2 + m_N^2) A_S^{I,J}(s) + m_N (s + m_\pi^2 - m_N^2) B_S^{I,J}(s) \right] \end{aligned} \quad (29)$$

with

$$F_{C/S}^{I,J}(s) = \frac{1}{32\pi} \int_{-1}^1 dz_s F^I(s, t) [P_{J+1/2}(z_s) \pm P_{J-1/2}(z_s)], \quad F = A, B \quad (30)$$

$z_s = \cos \theta$ with θ the scattering angle in center of mass frame (CM). The PWAs $T_{\pm}^{I,J}$ satisfy unitarity condition:

$$\text{Im} T_{\pm}^{I,J}(s) = \rho(s, m_\pi, m_N) |T_{\pm}^{I,J}(s)|^2, \quad s > s_R = (m_\pi + m_N)^2. \quad (31)$$

In this manuscript, the full amplitudes of πN scatterings are calculated within LSM. At tree level, there are three diagrams as depicted in FIG. 4.

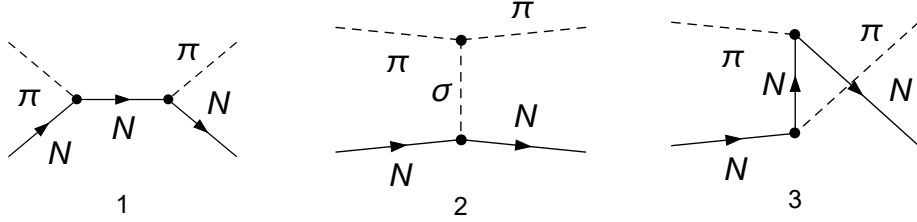


FIG. 4: The tree-level Feynman diagrams contributing to πN scatterings.

Contributions to invariant amplitudes $A^{1/2}(s, t, u)$ and $B^{1/2}(s, t, u)$ at tree level read

$$\begin{aligned} A^{1/2}(s, t, u) &= -\frac{g\lambda v}{3(t - m_\sigma^2)}, \\ B^{1/2}(s, t, u) &= -g^2 \left(\frac{3}{s - m_N^2} + \frac{1}{u - m_N^2} \right). \end{aligned} \quad (32)$$

According to Eq. (30), after partial-wave projection, the expressions of $A_{C/S}^{1/2,1/2}$ and $B_{C/S}^{1/2,1/2}$ are listed as follows,

$$A_C^{1/2,1/2}(s) = -\frac{g\lambda v}{96\pi k^2} \left(1 - \frac{(m_\sigma^2 + 4k^2)I(s)}{4k^2} \right), \quad (33)$$

$$A_S^{1/2,1/2}(s) = -\frac{g\lambda v}{96\pi k^2} \left(1 - \frac{m_\sigma^2 I(s)}{4k^2} \right), \quad (34)$$

$$B_C^{1/2,1/2}(s) = \frac{g^2}{32\pi} \left(-\frac{6}{s - m_N^2} + \frac{1}{k^2} - \frac{m_N^2 (s - c_L) \ln\left(\frac{s - c_R}{m_N^2 (s - c_L)}\right)}{4sk^4} \right), \quad (35)$$

$$B_S^{1/2,1/2}(s) = \frac{g^2}{32\pi} \left(\frac{6}{s - m_N^2} + \frac{1}{k^2} - \frac{(s - c_R) \ln\left(\frac{s(s-c_R)}{m_N^2(s-c_L)}\right)}{4k^4} \right), \quad (36)$$

with $k = \sqrt{s}\rho(s, m_\pi, m_N)/2$ being the magnitude of 3-momentum in CM and

$$I(s) = \ln \left(\frac{((m_\pi^2 - m_N^2)^2 - 2s(m_\pi^2 + m_N^2) + s(s + m_\sigma^2))}{m_\sigma^2 s} \right). \quad (37)$$

$B_C(s)$ and $B_S(s)$ contain the u -cut in the interval ($c_L = (m_N^2 - m_\pi^2)^2/m_N^2$, $c_R = m_N^2 + 2m_\pi^2$) from the logarithmic term generated by u -channel nucleon exchange, as depicted in the 3rd diagram in Fig. 4. When $2m_\pi < m_\sigma < 2m_N$, the $I(s)$ function contains circular arc cuts[8] centered at the origin with a radius of $m_N^2 - m_\pi^2$. At one loop, the circular cut emerges due to continuous two-particle spectrum, which covers the circular arc cut.

After partial-wave projection, the perturbative PWAs will be unitarized by N/D method⁶, which means to solve an integral equation about $N(s)$ function:

$$N(s) = N(s_0) + U(s) - U(s_0) + \frac{(s - s_0)}{\pi} \int_{s_R}^{\infty} \frac{(U(s) - U(s'))\rho(s', m_\pi, m_N)N(s')}{(s' - s_0)(s' - s)} ds'. \quad (38)$$

The subtraction point s_0 and subtraction value $N(s_0)$ can be chosen appropriately and $U(s)$ function should be analytic when $s > s_R$, such that $N(s)$ only contains left hand cuts

$$U(s) - U(s') = \frac{s - s'}{2\pi i} \int_L \frac{\text{disc } M(\tilde{s})}{(\tilde{s} - s)(\tilde{s} - s')} d\tilde{s}, \quad (39)$$

where the subscript L denotes the left-hand cut where the integration is performed. The discontinuity of the amplitude $M(s)$ need to be an input from the perturbation calculation. Since the dispersion relation of the amplitude on the left-hand cut essentially gives the amplitude with the right-hand cut integral subtracted up to a polynomial, we can use the perturbative amplitude with the right-hand cut dispersion integral subtracted to estimate $U(s) - U(s')$ directly in the following.

The amplitude satisfying the unitarity condition can be constructed as (we use $M(s)$ to represent πN scattering amplitude in S_{11} channel):

$$\begin{aligned} M(s) &= \frac{N(s)}{D(s)}, \\ D(s) &= 1 - \frac{s - s_0}{\pi} \int_{s_R}^{\infty} \frac{\rho(s')N(s')}{(s' - s)(s' - s_0)} ds'. \end{aligned} \quad (40)$$

One can numerically solve the equation by inverse matrix method, after introducing a cutoff Λ such that the integral interval becomes (s_R, Λ) instead of (s_R, ∞) . In the following, s_0, m_σ and Λ , are fixed at $s_R, 0.55\text{GeV}^2$ and $(m_N + m_\sigma)^2$, respectively.

At tree level, since there is already no right-hand cut in M_t , we set $U(s)$ equal to tree-level amplitude $M_t(s)$, and $N(s_0)$ equal to $M_t(s_0)$. At one-loop level, parameter $N(s_0)$ is set equal to $M_t(s_0) + M_l(s_0)$ and $U(s)$ is written as:

$$U(s) = M_t(s) + M_l(s) - \frac{s}{\pi} \int_{s_R} \frac{\rho(s', m_\pi, m_N)M_t^2(s')}{s'(s' - s)}, \quad (41)$$

with $M_l(s)$ the one-loop correction to the PWA. The full one-loop amplitude has been known for a long time [36], and after partial wave projection, the PWA is too long to be presented here⁸. The third term in the above expression ensures $U(s)$ to be analytic in the interval $(s_R, (m_M + m_\sigma)^2)$ according to perturbative unitarity:

$$\text{Im } M_l(s) = \rho(s, m_\pi, m_N)|M_t(s)|^2, \quad s > s_R. \quad (42)$$

There still exists cuts above $(m_\sigma + m_N)^2$ in real axis, but we fix the cutoff $\Lambda = (m_N + m_\sigma)^2$ such that the unitarized amplitude satisfies unitarity condition in the interval $(s_R, (m_N + m_\sigma)^2)$.

⁶ Here N/D method is used to avoid spurious poles which may present in the amplitude using Padé approximation.

⁷ Here the m_σ is chosen slightly different from $\pi\pi$ case, since the $N^*(920)$ pole is close to the Roy-equation result with this choice.

⁸ The code is also available upon request.

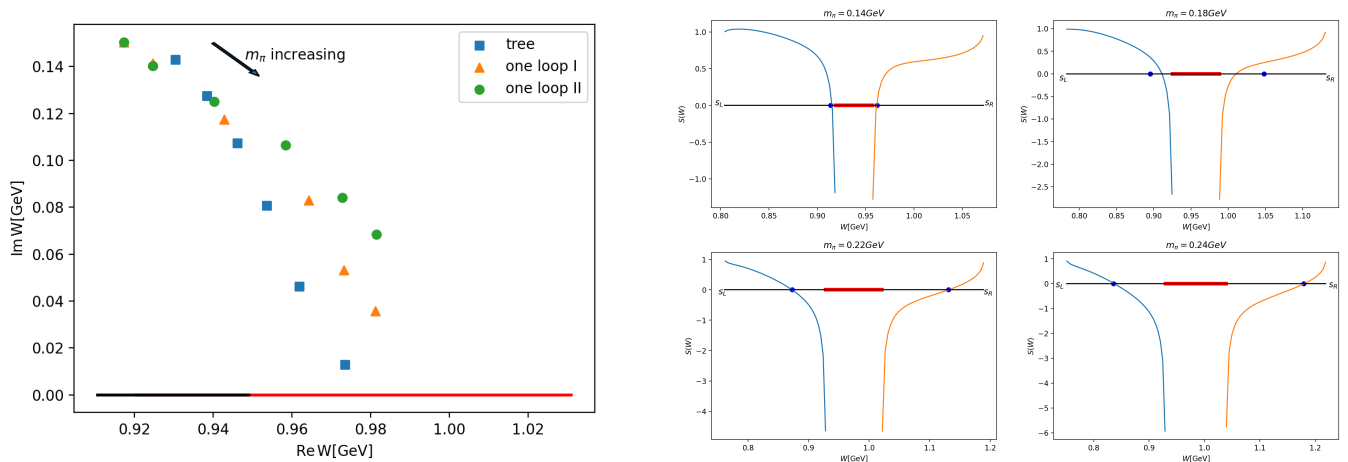


FIG. 5: Left: the trajectories of $N^*(920)$ pole with m_π variation from 0.140GeV to 0.240GeV with step 0.02GeV. The black and red straight lines denote the u -cuts with $m_\pi = 0.140\text{GeV}$ and 0.240GeV, respectively. Right: the values of S matrix at one-loop level in intervals (c_L, s_L) and (c_R, s_R) on the first Riemann sheet. The red lines denote u -cuts and endpoints of black lines are s_L and s_R , respectively. The blue intersection points represent virtual states.

A pole at $(0.92 - 0.15i)\text{GeV}$ for the one-loop order and $(0.93 - 0.14i)\text{GeV}$ for the tree level corresponding to $N^*(920)$ can be found on the second sheet with physical pion and nucleon masses. The pole trajectories of $N^*(920)$ for the tree-level and the one-loop level amplitude as m_π increases are shown in FIG. 5. At the one-loop order, we also calculate the trajectories with fixed λ labeled by “one loop II” in FIG. 5, beside the one with fixed m_σ labeled by “one loop I”. The imaginary part of $N^*(920)$ decreases while the real part grows when m_π increases in all cases, causing the pole to move toward the u -cuts between the two branch points at c_R and c_L . The real part of the pole at one-loop level increases faster than the one at tree level. Finally, when further increasing m_π , the $N^*(920)$ pole will disappear on RSII.

We also studied the behavior of the two virtual states [37] lying in the interval $(s_L = (m_N - m_\pi)^2, c_L)$ and (c_R, s_R) , respectively. The values of S matrix calculated with one-loop level input in the two intervals on the first Riemann sheet are plotted in FIG.5, which demonstrates the fact that the S matrix equals to unity at s_L and s_R by definition while it tends to negative infinity when s is close to the two branch points c_L and c_R . As a result, a zero point inside each interval occurs. The calculation reveals that the virtual states move towards s_R or s_L with increasing m_π .

IV. DISCUSSIONS AND CONCLUSIONS

In this paper we have studied the σ pole trajectory and the $N^*(920)$ pole trajectory with varying m_π , in a linear σ model with nucleons, aided by certain unitarization approximations. The m_π dependence of f_π from the Lattice results is also taken into account, which renders the LSM more reasonable in approximating the low energy QCD. The σ pole trajectory is found to be in agreement with previous studies [15, 16]. The result on $N^*(920)$ pole trajectory is novel. The $N^*(920)$ pole is found to move towards the u -cut on the real axis on the second Riemann sheet with increasing m_π . This result is also in qualitative agreement with that obtained in a chiral perturbation theory with nucleons (to be presented elsewhere). The next interesting topic for future studies would be to investigate the $N^*(920)$ pole trajectory in the presence of temperature and chemical potential, and the old concept of parity doublet model may return with some new ingredients.

ACKNOWLEDGMENTS

This work is supported by China National Natural Science Foundation under Contract No. 12335002, 12375078. This work is also supported by “the Fundamental Research Funds for the Central Universities”.

Appendix A: The expressions of counter terms and renormalization constants

The counter terms and renormalization constants take following forms up to one-loop level,

$$Z_\phi = 1 - \frac{g^2}{4\pi^2} (B_0(m_\pi^2, m_N^2, m_N^2) + m_\pi^2 B'_0(m_\pi^2, m_N^2, m_N^2)) - \frac{\lambda^2 v^2}{144\pi^2} B'_0(m_\pi^2, m_\pi^2, m_\sigma^2), \quad (\text{A1})$$

$$Z_F = 1 - \frac{g^2}{32\pi^2 m_N^2} (3m_\pi^2 B_0(m_N^2, m_\pi^2, m_N^2) + m_\sigma^2 B_0(m_N^2, m_N^2, m_\sigma^2) - 3A_0(m_\pi^2) + 4A_0(m_N^2) - A_0(m_\sigma^2)) \\ + \frac{g^2}{16\pi^2} (3m_\pi^2 B'_0(m_N^2, m_\pi^2, m_N^2) + m_\sigma^2 B'_0(m_N^2, m_N^2, m_\sigma^2) - 4m_N^2 B'_0(m_N^2, m_N^2, m_\sigma^2)), \quad (\text{A2})$$

$$Z_g = 1 + \frac{g^2}{16\pi^2 m_N^2} (-3m_\pi^2 B_0(m_N^2, m_\pi^2, m_N^2) - m_\sigma^2 B_0(m_N^2, m_N^2, m_\sigma^2) + 3A_0(m_\pi^2) - 4A_0(m_N^2) + A_0(m_\sigma^2)) \\ + \frac{g^2}{16\pi^2} (2B_0(m_N^2, m_N^2, m_\sigma^2) + 3m_\pi^2 B'_0(m_N^2, m_\pi^2, m_N^2) + m_\sigma^2 B'_0(m_N^2, m_N^2, m_\sigma^2) - 4m_N^2 B'_0(m_N^2, m_N^2, m_\sigma^2)), \quad (\text{A3})$$

$$\delta m_\pi^2 = \frac{\lambda^2 v^2}{144\pi^2} (B_0(m_\pi^2, m_\pi^2, m_\sigma^2) - m_\pi^2 B'_0(m_\pi^2, m_\pi^2, m_\sigma^2)) + \frac{\lambda}{96\pi^2} (5A_0(m_\pi^2) + A_0(m_\sigma^2)) \\ - \frac{g^2}{4\pi^2} (m_\pi^4 B'_0(m_\pi^2, m_N^2, m_N^2) + 2A_0(m_N^2)), \quad (\text{A4})$$

$$\delta m_\sigma^2 = \frac{\lambda^2 v^2}{\pi^2} \left(\frac{\text{Re } B_0(m_\sigma^2, m_\pi^2, m_\pi^2)}{96} + \frac{B_0(m_\sigma^2, m_\sigma^2, m_\sigma^2)}{32} - \frac{m_\sigma^2 B'_0(m_\pi^2, m_\pi^2, m_\sigma^2)}{144} \right) + \frac{\lambda}{32\pi^2} (A_0(m_\pi^2) + A_0(m_\sigma^2)) \\ - \frac{g^2 m_\sigma^2}{4\pi^2} (B_0(m_\pi^2, m_N^2, m_N^2) - B_0(m_\sigma^2, m_N^2, m_N^2) + m_\pi^2 B'_0(m_\pi^2, m_N^2, m_N^2)) - \frac{g^2}{4\pi^2} (2A_0(m_N^2) \\ + 4m_N^2 B_0(m_\sigma^2, m_N^2, m_N^2)). \quad (\text{A5})$$

The definitions of 1-point function $A_0(m^2)$ and 2-point function $B_0(p^2, m_1^2, m_2^2)$ are expressed

$$A_0(m^2) \equiv -16\pi^2 i \int \frac{d^4 k}{(2\pi)^4} \frac{1}{k^2 - m^2}, \quad (\text{A6}) \\ B_0(p^2, m_1^2, m_2^2) \equiv -16\pi^2 i \int \frac{d^4 k}{(2\pi)^4} \frac{1}{(k^2 - m_1^2)[(p+k)^2 - m_2^2]}.$$

B'_0 denotes the derivation with respect to the first argument.

-
- [1] Y.-F. Wang, D.-L. Yao, and H.-Q. Zheng, *Eur. Phys. J. C* **78**, 543 (2018), arXiv:1712.09257 [hep-ph].
[2] Y.-F. Wang, D.-L. Yao, and H.-Q. Zheng, *Chin. Phys. C* **43**, 064110 (2019), arXiv:1811.09748 [hep-ph].
[3] H. Q. Zheng, Z. Y. Zhou, G. Y. Qin, Z. Xiao, J. J. Wang, and N. Wu, *Nucl. Phys. A* **733**, 235 (2004), arXiv:hep-ph/0310293.
[4] Z. Y. Zhou and H. Q. Zheng, *Nucl. Phys. A* **775**, 212 (2006), arXiv:hep-ph/0603062.
[5] Z. Y. Zhou, G. Y. Qin, P. Zhang, Z. Xiao, H. Q. Zheng, and N. Wu, *JHEP* **02**, 043, arXiv:hep-ph/0406271.
[6] Z. Xiao and H. Q. Zheng, *Nucl. Phys. A* **695**, 273 (2001), arXiv:hep-ph/0011260.
[7] J. He, Z. Xiao, and H. Q. Zheng, *Phys. Lett. B* **536**, 59 (2002), [Erratum: *Phys.Lett.B* 549, 362–363 (2002)], arXiv:hep-ph/0201257.
[8] Y. Ma, W.-Q. Niu, Y.-F. Wang, and H.-Q. Zheng, *Commun. Theor. Phys.* **72**, 105203 (2020), arXiv:2002.02351 [hep-ph].
[9] Q.-Z. Li, Y. Ma, W.-Q. Niu, Y.-F. Wang, and H.-Q. Zheng, *Chinese Physics C* **46**, 023104 (2022).
[10] X.-H. Cao, Q.-Z. Li, and H.-Q. Zheng, *JHEP* **12**, 073, arXiv:2207.09743 [hep-ph].
[11] M. Hoferichter, J. R. de Elvira, B. Kubis, and U.-G. Meißner, *Phys. Lett. B* **853**, 138698 (2024), arXiv:2312.15015 [hep-ph].

- [12] Y. Ma, W.-Q. Niu, D.-L. Yao, and H.-Q. Zheng, *Chin. Phys. C* **45**, 014104 (2021), arXiv:2005.10695 [hep-ph].
- [13] C. Hanhart, J. R. Pelaez, and G. Rios, *Phys. Rev. Lett.* **100**, 152001 (2008), arXiv:0801.2871 [hep-ph].
- [14] X.-L. Gao, Z.-H. Guo, Z. Xiao, and Z.-Y. Zhou, *Phys. Rev. D* **105**, 094002 (2022), arXiv:2202.03124 [hep-ph].
- [15] X.-H. Cao, Q.-Z. Li, Z.-H. Guo, and H.-Q. Zheng, *Phys. Rev. D* **108**, 034009 (2023), arXiv:2303.02596 [hep-ph].
- [16] Y.-L. Lyu, Q.-Z. Li, Z. Xiao, and H.-Q. Zheng, *Phys. Rev. D* **109**, 094026 (2024), arXiv:2402.19243 [hep-ph].
- [17] Y.-L. Lyu, Q.-Z. Li, Z. Xiao, and H.-Q. Zheng, *Phys. Rev. D* **110**, 094054 (2024), arXiv:2405.11313 [hep-ph].
- [18] Z.-H. Guo, L. Y. Xiao, and H. Q. Zheng, *Int. J. Mod. Phys. A* **22**, 4603 (2007), arXiv:hep-ph/0610434.
- [19] Z. H. Guo, J. J. Sanz Cillero, and H. Q. Zheng, *JHEP* **06**, 030, arXiv:hep-ph/0701232.
- [20] Z. H. Guo, J. J. Sanz-Cillero, and H. Q. Zheng, *Phys. Lett. B* **661**, 342 (2008), arXiv:0710.2163 [hep-ph].
- [21] M. Gell-Mann and M. Levy, *Nuovo Cim.* **16**, 705 (1960).
- [22] J. A. Mignaco and E. Remiddi, *Nuovo Cim. A* **1**, 376 (1971).
- [23] B. W. Lee, *Nucl. Phys. B* **9**, 649 (1969).
- [24] M. Niehus, M. Hoferichter, B. Kubis, and J. Ruiz de Elvira, *Phys. Rev. Lett.* **126**, 102002 (2021), arXiv:2009.04479 [hep-ph].
- [25] M. Gong *et al.* (XQCD), *Phys. Rev. D* **88**, 014503 (2013), arXiv:1304.1194 [hep-ph].
- [26] C. Alexandrou, M. Constantinou, S. Dinter, V. Drach, K. Hadjiyiannakou, K. Jansen, G. Koutsou, and A. Vaquero, *Phys. Rev. D* **91**, 094503 (2015), arXiv:1309.7768 [hep-lat].
- [27] A. Walker-Loud, *PoS LATTICE2013*, 013 (2014), arXiv:1401.8259 [hep-lat].
- [28] A. Gasparyan and M. F. M. Lutz, *Nucl. Phys. A* **848**, 126 (2010), arXiv:1003.3426 [hep-ph].
- [29] J. Gasser and H. Leutwyler, *Phys. Rept.* **87**, 77 (1982).
- [30] S. Steininger, U.-G. Meissner, and N. Fettes, *JHEP* **09**, 008, arXiv:hep-ph/9808280.
- [31] A. Rodas, J. J. Dudek, and R. G. Edwards (Hadron Spectrum), *Phys. Rev. D* **109**, 034513 (2024), arXiv:2304.03762 [hep-lat].
- [32] A. Rodas, J. J. Dudek, and R. G. Edwards (Hadron Spectrum), *Phys. Rev. D* **108**, 034513 (2023), arXiv:2303.10701 [hep-lat].
- [33] G.-Y. Qin, W. Z. Deng, Z. Xiao, and H. Q. Zheng, *Phys. Lett. B* **542**, 89 (2002), arXiv:hep-ph/0205214.
- [34] J. I. Basdevant and B. W. Lee, *Phys. Rev. D* **2**, 1680 (1970).
- [35] X.-H. Cao, Y. Ma, and H.-Q. Zheng, *Phys. Rev. D* **103**, 114007 (2021), arXiv:2101.12576 [nucl-th].
- [36] J. A. Mignaco and E. Remiddi, *Nuovo Cim. A* **1**, 395 (1971).
- [37] Q.-Z. Li and H.-Q. Zheng, *Commun. Theor. Phys.* **74**, 115203 (2022), arXiv:2108.03734 [nucl-th].